

Short Communication

## Influence of CeO<sub>2</sub> Nanoparticles on Structure and Properties of Anodic Oxide Film on 2024 Aluminum Alloy

Xiaokun Li<sup>1,2,\*</sup>, Xin Liu<sup>3</sup>

<sup>1</sup> School of Environment Engineering, Yellow River Conservancy Technical Institute, Kaifeng 475004, China

<sup>2</sup> Henan Engineering Technology Research Center of Green Coating Materials, Kaifeng 475004, China

<sup>3</sup> School of Environmental Science and Engineering, Suzhou University of Science and Technology, Suzhou 215009, China

\*E-mail: [li\\_kaifeng004@163.com](mailto:li_kaifeng004@163.com)

Received: 2 January 2022 / Accepted: 19 February 2022 / Published: 5 April 2022

---

2024 aluminum alloy was used as the substrate to prepare an anodic oxide film from sulfuric acid electrolyte containing CeO<sub>2</sub> nanoparticles with different concentrations. The influence of concentration of CeO<sub>2</sub> nanoparticles on the morphology, component, phase composition, microhardness, surface wettability and corrosion resistance of anodic oxide film was studied. The results show that adding proper amount of CeO<sub>2</sub> nanoparticles can play the role of shielding and filling, which is beneficial to improve the surface smoothness and compactness of anodic oxide film, and thus improve its properties. When the concentration of CeO<sub>2</sub> nanoparticles is 2.5 g/L, the porosity of the anodic oxide film is only 16.4%, showing compact surface. The anodic oxide film is composed of Al, O, S and Ce elements with  $\alpha$ -Al<sub>2</sub>O<sub>3</sub> and  $\gamma$ -Al<sub>2</sub>O<sub>3</sub> phases, and exhibits superhydrophobic state with better corrosion resistance and higher microhardness.

---

**Keywords:** anodic oxide film; CeO<sub>2</sub> nanoparticles; microhardness; surface wettability; corrosion resistance

### 1. INTRODUCTION

Although aluminum alloy has good self-passivation performance in a conventional atmospheric environment to form a natural passivation film, but this film is not continuous and its protective effect is limited. The corrosion resistance of aluminum alloy can be improved obviously by anodic oxidation technique. Among them, sulfuric acid anodic oxidation is most commonly used [1-4]. However, due to the strong acid and dissolution of sulfuric acid electrolyte, the anodic oxide film is easy to be dissolved resulting in the decrease of corrosion resistance. Therefore, weakening the corrosion dissolving effect of sulfuric acid electrolyte during anodic oxidation process is beneficial to improve the corrosion

resistance of anodic oxide film, thus prolonging its service life. It was found that organic acids such as malic acid, citric acid and tartaric acid added to sulfuric acid electrolyte could inhibit corrosion, weaken the dissolution degree of anodic oxide film, and facilitate the formation of anodic oxide film possessing dense surface and good corrosion resistance [5-9].

Rare earth, metal or oxide particles are often used to prepare functional and composite materials. If rare earth, metal or oxide particles are added into acid electrolyte to participate in the anodic oxidation process, it is also expected to weaken the corrosion dissolution degree of anodic oxidation film, so as to further improve the corrosion resistance of anodic oxidation film [10-16]. In this paper, CeO<sub>2</sub> nanoparticles were added into sulfuric acid electrolyte to prepare anodic oxide film on the surface of 2024 aluminum alloy. The influence of concentration of CeO<sub>2</sub> nanoparticles on the morphology, structure, microhardness, surface wettability and corrosion resistance of anodic oxide film was studied.

## 2. EXPERIMENTAL

### 2.1 Substrate and pretreatment

The substrate was 2024 aluminum alloy which was cut into 40 mm×24 mm×1 mm samples. The surface was polished step by step with 1000<sup>#</sup> and 2000<sup>#</sup> sandpaper until getting smooth surface. Then, the surface was cleaned by ultrasonic wave in the solution with acetone and deionized water at room temperature (ultrasonic power 120 W, 5 min respectively). After that, the substrate was activated with dilute nitric acid solution (volume fraction 20%), and finally cleaned by deionized water.

### 2.2 Preparation of anodic oxide film

Pure sulfuric acid electrolyte (98% concentrated sulfuric acid 180 g/L) was used, and CeO<sub>2</sub> nanoparticles with different concentrations (0 g/L, 1.2 g/L, 2.5 g/L, 4 g/L) were added during anodic oxidation process. The solution was oscillated by ultrasonic wave for 2 h, and followed by magnetic stirring for 6 h to ensure that the CeO<sub>2</sub> nanoparticles were fully wetted and evenly dispersed in the electrolyte. The pretreated aluminum alloy sample was used as the anode, and the pure lead plate was used as the cathode. The current density was set at 2 A/dm<sup>2</sup>. The temperature of electrolyte was kept at 24 °C by water bath heating to do the anodic oxidation experiment for 45 min.

### 2.3 Properties testing

#### 2.3.1 Surface morphology and component

The morphology and component of 2024 aluminum alloy and different anodic oxide films were characterized by scanning electron microscopy (SUPRA55, ZEISS, Germany) and energy dispersive spectroscopy (X-MAX80, OXFORD, UK) respectively. In addition, the image processing software

was used to transform the format, remove the noise and adjust the threshold of the image taken by the scanning electron microscope. The characteristics of the holes and cracks were extracted and filled with red. The porosity of different anodic oxide films was estimated according to the percentage of red area.

### 2.3.2 Structure characterization

X-ray diffractometer (D8 Advance, BRUKER, Germany) and Jade software were used to characterization and analyze the phase composition of different anodic oxide films. The scanning rate was 4°/min, from 20° to 90°.

### 2.3.3 Thickness measurement

The thickness of different anodic oxide films was measured by high precision thickness gauge with digital display (STT-450, Beijing Zhongjiaotong Engineering Instrument Institute, China). In order to reduce the error, each sample was measured at three different locations and the results were averaged.

### 2.3.4 microhardness testing

Vickers microhardness tester (HV-1000, Beijing Times Create He Technology Co., LTD.) was used to test the microhardness of 2024 aluminum alloy and different anodic oxide films. A load of 50 g was applied for 15 s. In order to reduce the error, five points were selected on the surface of each sample, and the results were averaged.

### 2.3.5 Surface wettability

The water droplet contact angle of 2024 aluminum alloy and different anodic oxide films were measured by a contact angle meter (DSA30, KRUSS, Germany). Water droplet with a volume of 4  $\mu$ L was dropped at three different positions on the sample surface, and the measurement results were averaged. When the water droplet contact angle is lower than 90°, it indicates that the surface is hydrophilic. When the water droplet contact angle is between 90° and 150°, it indicates that the surface is hydrophobic. When the water droplet contact angle is between 150° and 180°, it indicates that the surface is superhydrophobic.

### 2.3.6 Corrosion resistance testing

The polarization curves of 2024 aluminum alloy and different anodic oxide films were measured by CHI760 electrochemical workstation. The sample to be tested was as the working

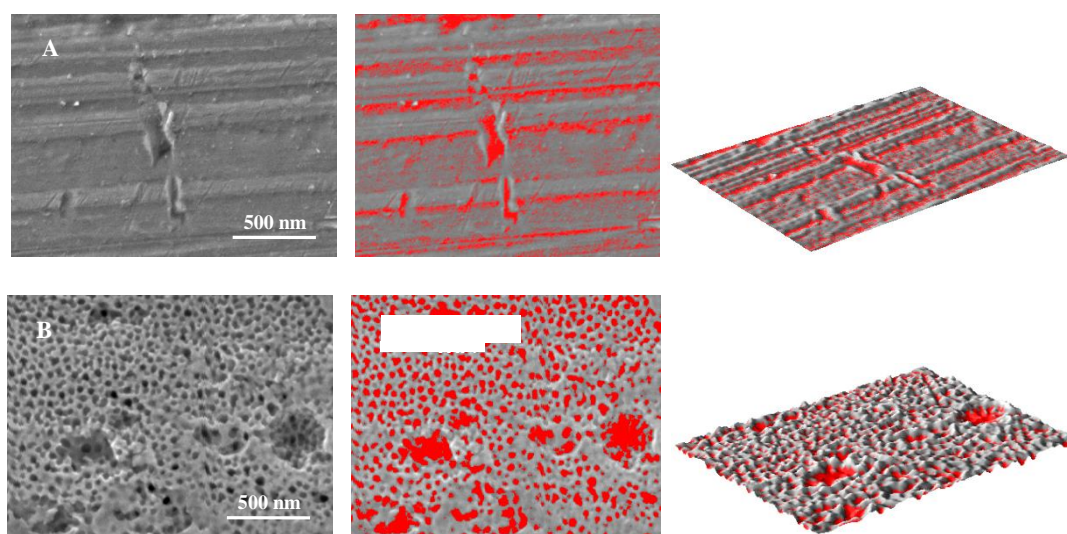
electrode while platinum plate and saturated calomel electrode were as the auxiliary electrode and reference electrode, respectively. The corrosion medium is 3.5% sodium chloride solution with 1 mV/s scanning rate.

The corrosion resistance of 2024 aluminum alloy and different anodic oxide films were further evaluated by full immersion testing in 3.5% sodium chloride solution for 15 days at room temperature. After the experiment, the samples were cleaned with normal temperature deionized water and then dried. The corrosion morphology was observed by scanning electron microscope.

### 3. RESULTS AND DISCUSSION

#### 3.1 Influence of concentration of $CeO_2$ nanoparticles on morphology and component of anodic oxide film

Figure 1 shows the morphology characteristics of 2024 aluminum alloy and different anodic oxide films. The prepared anodic oxide films with and without  $CeO_2$  nanoparticles are all completely covered with porous alumina which is also reported in some papers [17-20]. However, in the condition of without  $CeO_2$  nanoparticles, there are more irregular pits on the surface of anodic oxide film possessing 27.1% porosity resulting in poor surface smoothness and compactness. The addition of  $CeO_2$  nanoparticles reduces the degree of concavity and irregular pits on the anodic oxide film surface. The reason is that the participation of  $CeO_2$  nanoparticles in the anodic oxidation process can play the role of homogenizing current distribution and shielding, avoid local over-dissolution of anodic oxide film, and can fill holes to a certain extent to improve the surface smoothness and compactness of anodic oxide film.



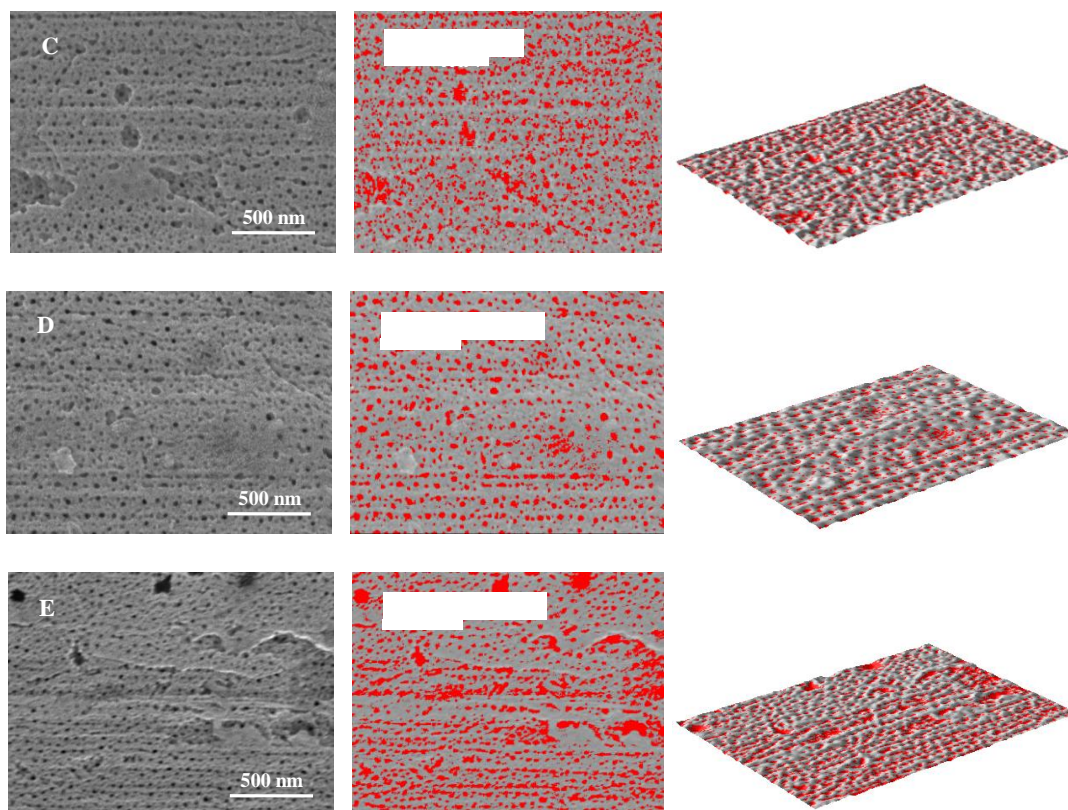


**Figure 1.** Morphology characteristics of 2024 aluminum alloy and different anodic oxide films; A-2024 aluminum alloy; B-anodic oxide film (concentration of CeO<sub>2</sub> nanoparticles is 0 g/L); C-anodic oxide film (concentration of CeO<sub>2</sub> nanoparticles is 1.2 g/L); D-anodic oxide film (concentration of CeO<sub>2</sub> nanoparticles is 2.5 g/L); E-anodic oxide film (concentration of CeO<sub>2</sub> nanoparticles is 4 g/L)

When the concentration of CeO<sub>2</sub> nanoparticles is 2.5 g/L, the surface roughness and density of anodic oxide film are the lowest, and the porosity is only 16.4%, which is obviously better than that of the anodic oxide film prepared without CeO<sub>2</sub> nanoparticles. However, when the concentration of CeO<sub>2</sub> nanoparticles is too high, the influence of particle agglomeration phenomenon is not beneficial and significant to prevent local over-dissolution of anodic oxide film leading to increase of porosity. Figure 2 shows the component of different anodic oxide films. The component of anodic oxide film prepared without CeO<sub>2</sub> nanoparticles is Al, O and S elements, and the mass fraction of Al and O elements is close to each other. The element S in the anodic oxide film is due to the participation of sulfate ions in the electrolyte (98% concentrated sulphuric acid 180 g/L) during anodic oxidation process. When the concentration of CeO<sub>2</sub> nanoparticles is from 1.2 g/L~4 g/L, the component of the prepared anodic oxide film is Al, O, S and Ce elements, which indicates that CeO<sub>2</sub> nanoparticles participate in the anodic oxidation process and enter into the anodic oxide film. The higher the mass fraction of Ce element is, the more CeO<sub>2</sub> nanoparticles enter the anodic oxide film, which is beneficial to improve the properties of anodic oxide film.

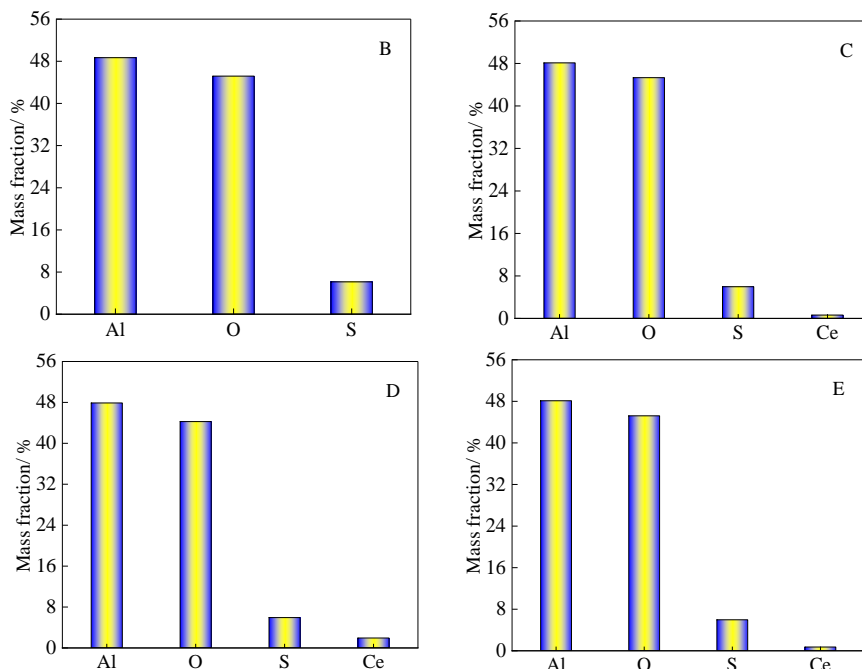


**Figure 2.** Component of different anodic oxide films; B-anodic oxide film (concentration of CeO<sub>2</sub> nanoparticles is 0 g/L); C-anodic oxide film (concentration of CeO<sub>2</sub> nanoparticles is 1.2 g/L); D-anodic oxide film (concentration of CeO<sub>2</sub> nanoparticles is 2.5 g/L); E-anodic oxide film (concentration of CeO<sub>2</sub> nanoparticles is 4 g/L)

### 3.2 Influence of concentration of CeO<sub>2</sub> nanoparticles on structure of anodic oxide film

Figure 3 shows X-ray diffraction spectra of different anodic oxide films. It can be seen that different anodic oxide films all show diffraction peaks of Al,  $\alpha$ -Al<sub>2</sub>O<sub>3</sub> and  $\gamma$ -Al<sub>2</sub>O<sub>3</sub> phases, and the positions of each diffraction peak are almost the same. After deducting the Al phase of matrix, it can be inferred that different anodic oxide films are composed of  $\alpha$ -Al<sub>2</sub>O<sub>3</sub> and  $\gamma$ -Al<sub>2</sub>O<sub>3</sub> phases [21-23], indicating that the concentration of CeO<sub>2</sub> nanoparticles has no influence on the phase composition of anodic oxide films.

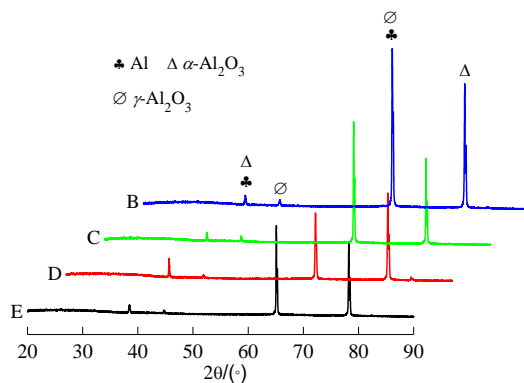


**Figure 3.** X-ray diffraction pattern of different anodic oxide films; B-anodic oxide film (concentration of CeO<sub>2</sub> nanoparticles is 0 g/L); C-anodic oxide film (concentration of CeO<sub>2</sub> nanoparticles is 1.2 g/L); D-anodic oxide film (concentration of CeO<sub>2</sub> nanoparticles is 2.5 g/L); E-anodic oxide film (concentration of CeO<sub>2</sub> nanoparticles is 4 g/L)

### 3.3 Influence of concentration of CeO<sub>2</sub> nanoparticles on microhardness of anodic oxide film

As shown in Figure 4, the thickness of anodic oxide film prepared without CeO<sub>2</sub> nanoparticles is about 14.6 μm and the microhardness is 306.8 HV. When the concentration of CeO<sub>2</sub> nanoparticles is from 1.2 g/L~4 g/L, the thickness of anodic oxide film decreases gradually, whereas the microhardness increases firstly and then decreases. When the concentration of CeO<sub>2</sub> nanoparticles is 2.5 g/L, the microhardness of anodic oxide film is the largest, reaching to 348.5 HV, which is three times larger than the microhardness of 2024 aluminum alloy. Combined with the above mentioned, adding an appropriate amount of CeO<sub>2</sub> nanoparticles can improve the compactness of anodic oxide film, enhances the overall bearing capacity and resistance to local plastic deformation, and thus has a high microhardness. However, when the concentration of CeO<sub>2</sub> nanoparticles is too high, the compactness of anodic oxide film decreases due to the agglomeration phenomenon of nanoparticles caused by size effect and surface tension effect. The overall bearing capacity and resistance to local plastic deformation are weakened, so the microhardness of anodic oxide film decreases.

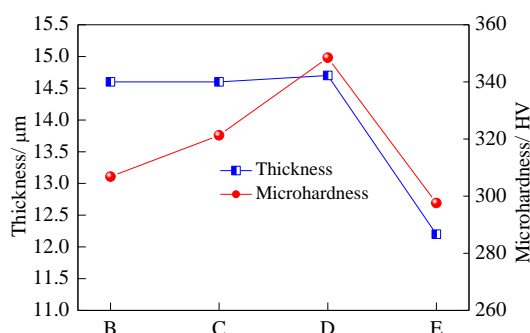
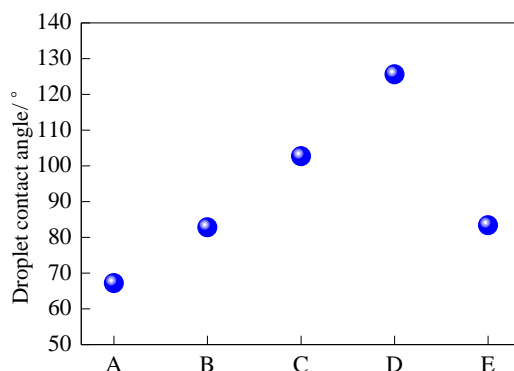


**Figure 4.** Thickness and microhardness of different anodic oxide films; B-anodic oxide film (concentration of CeO<sub>2</sub> nanoparticles is 0 g/L); C-anodic oxide film (concentration of CeO<sub>2</sub> nanoparticles is 1.2 g/L); D-anodic oxide film (concentration of CeO<sub>2</sub> nanoparticles is 2.5 g/L); E-anodic oxide film (concentration of CeO<sub>2</sub> nanoparticles is 4 g/L)

### 3.4 Influence of concentration of CeO<sub>2</sub> nanoparticles on surface wettability of anodic oxide film

Figure 5 shows the droplet contact angles of 2024 aluminum alloy and different anodic oxide films. It can be seen that the droplet contact angle of 2024 aluminum alloy is 67.2°, indicating that the surface is hydrophilic and water droplet are easy to spread out. The droplet contact angle of anodic oxide film prepared without CeO<sub>2</sub> nanoparticles is 82.8°, and the surface is also hydrophilic. When the concentration of CeO<sub>2</sub> nanoparticles is 2.5 g/L, the droplet contact angle of anodic oxide film is 125.6°, and the surface of anodic oxide film is hydrophobic. This indicates that adding proper amount of CeO<sub>2</sub> nanoparticles can change the wettability of anodic oxide film surface. The reason is that the participation of CeO<sub>2</sub> nanoparticles in anodic oxidation process can reduce the surface energy of anodic oxide film, weaken the affinity to water, and thus inhibit the spread of water droplet. The surface of anodic oxide film changes from hydrophilic to better hydrophobicity, which is beneficial to improve its corrosion resistance [24-26]. In our previous work, perfluorooctanoic acid and ammonium

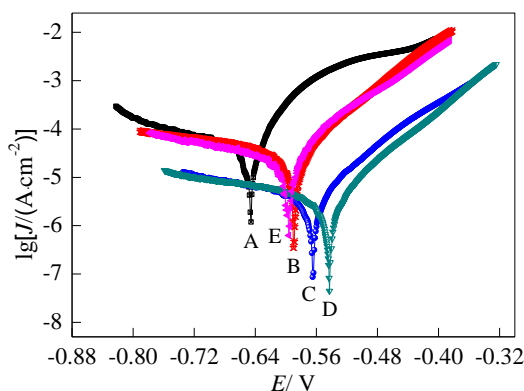
fluorotitanate were used to do surface modification for anodic oxide film on 2024 aluminum alloy, which has better corrosion resistance and larger droplet contact angle (approximate  $160^\circ$ ) [27]. However, the technology process is more complicated and the cost is higher than the work in this paper.



**Figure 5.** Droplet contact angle of 2024 aluminum alloy and different anodic oxide films; A-2024 aluminum alloy; B-anodic oxide film (concentration of  $\text{CeO}_2$  nanoparticles is 0 g/L); C-anodic oxide film (concentration of  $\text{CeO}_2$  nanoparticles is 1.2 g/L); D-anodic oxide film (concentration of  $\text{CeO}_2$  nanoparticles is 2.5 g/L); E-anodic oxide film (concentration of  $\text{CeO}_2$  nanoparticles is 4 g/L)

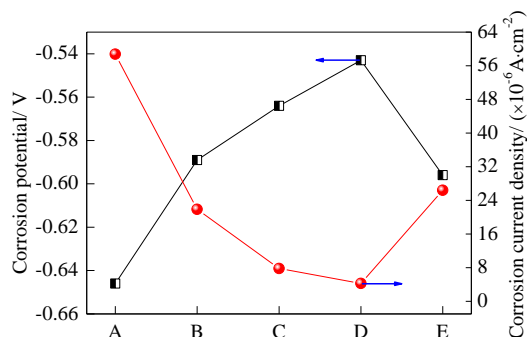
### 3.5 Influence of concentration of $\text{CeO}_2$ nanoparticles on corrosion resistance of anodic oxide film

Figure 6 shows the polarization curves of 2024 aluminum alloy and different anodic oxide films. As can be seen from Figure 6, the anodic oxide films prepared with and without  $\text{CeO}_2$  nanoparticles has more positive and smaller corrosion current density than that of 2024 aluminum alloy. In particular, when the concentration of  $\text{CeO}_2$  nanoparticles is 2.5 g/L, the anodic oxide film has the most positive corrosion potential and the lowest corrosion current density, which are  $-0.54$  V and  $4.26 \times 10^{-6}$  A/cm<sup>2</sup>, respectively, as shown in Figure 7.



**Figure 6.** Polarization curves of 2024 aluminum alloy and different anodic oxide films; A-2024 aluminum alloy; B-anodic oxide film (concentration of  $\text{CeO}_2$  nanoparticles is 0 g/L); C-anodic oxide film (concentration of  $\text{CeO}_2$  nanoparticles is 1.2 g/L); D-anodic oxide film (concentration of  $\text{CeO}_2$  nanoparticles is 2.5 g/L); E-anodic oxide film (concentration of  $\text{CeO}_2$  nanoparticles is 4 g/L)

According to the analysis above, the anodic oxide film prepared when the concentration of CeO<sub>2</sub> nanoparticles is 2.5 g/L has the lowest porosity, good compactness and strong resistance to the penetration of corrosive media, the corrosion tendency is very weak. In addition, CeO<sub>2</sub> nanoparticles can pay a shielding effect, at the same time to improve the anode oxide film surface wettability to present a better hydrophobicity which effectively reduces the contact area with the corrosive medium resulting in good corrosion resistance.



**Figure 7.** Corrosion potential and corrosion current density of 2024 aluminum alloy and different anodic oxide films; A-2024 aluminum alloy; B-anodic oxide film (concentration of CeO<sub>2</sub> nanoparticles is 0 g/L); C-anodic oxide film (concentration of CeO<sub>2</sub> nanoparticles is 1.2 g/L); D-anodic oxide film (concentration of CeO<sub>2</sub> nanoparticles is 2.5 g/L); E-anodic oxide film (concentration of CeO<sub>2</sub> nanoparticles is 4 g/L)

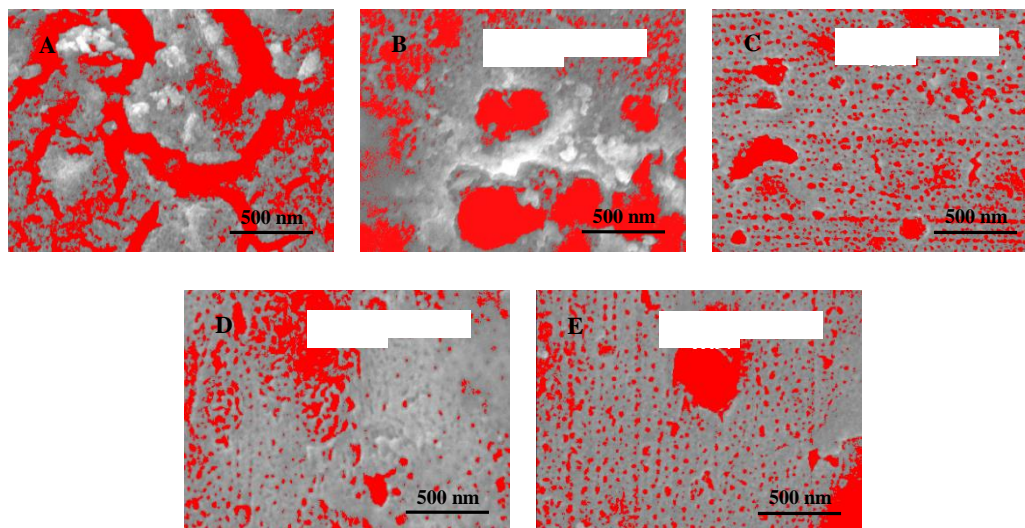


**Figure 8.** Corrosion morphology characteristics of 2024 aluminum alloy and different anodic oxide films; A-2024 aluminum alloy; B-anodic oxide film (concentration of CeO<sub>2</sub> nanoparticles is 0 g/L); C-anodic oxide film (concentration of CeO<sub>2</sub> nanoparticles is 1.2 g/L); D-anodic oxide film (concentration of CeO<sub>2</sub> nanoparticles is 2.5 g/L); E-anodic oxide film (concentration of CeO<sub>2</sub> nanoparticles is 4 g/L)

Figure 8 shows the corrosion morphology characteristics of 2024 aluminum alloy and different anodic oxide films after full immersion testing in 3.5% sodium chloride solution. It can be seen from

Figure 8 that 2024 aluminum alloy is severely corroded and has many deep corrosion pits on its surface, similar to the stepped morphology characteristics. The corrosion degree of the anodic oxide film prepared without CeO<sub>2</sub> nanoparticles is also serious presenting cracking phenomenon and corrosion with 34.5% porosity. When the concentration of CeO<sub>2</sub> nanoparticles is 1.2 g/L and 2.5 g/L, the corrosion degree of anodic oxide film is obviously reduced, and the porosity is 24.7% and 18.5%, respectively. However, when the concentration of CeO<sub>2</sub> nanoparticles is 4 g/L, the local corrosion pits are formed, and the porosity increases to 26.1%, indicating that the corrosion resistance becomes worse.

#### 4. CONCLUSIONS

(1) During anodic oxidation process, CeO<sub>2</sub> nanoparticles has no influence on the phase composition of anodic oxide film, but has a certain influence on the morphology and properties of anodic oxide film. The participation of appropriate CeO<sub>2</sub> nanoparticles in anodic oxidation process can homogenize current distribution, and fill holes to a certain extent, which is beneficial to improve the surface smoothness and compactness of anodic oxide film resulting in good surface wettability and better corrosion resistance.

(2) When the concentration of CeO<sub>2</sub> nanoparticles is 2.5 g/L, the anodic oxide film is composed of Al, O, S and Ce elements with  $\alpha$ -Al<sub>2</sub>O<sub>3</sub> and  $\gamma$ -Al<sub>2</sub>O<sub>3</sub> phases. The microhardness reaches 348.5HV, which is about three times of the microhardness of 2024 aluminum alloy. The corrosion current density decreased sharply, which can better protect 2024 aluminum alloy and delay corrosion.

#### ACKNOWLEDGMENT

This work is supported by Science and Technology Research Project of Kaifeng City (1901021) and University Key Scientific Research Project of Henan Province (20A530004).

#### References

1. W. Bensalah, M. Feki, M. Wery and H. F. Ayedi, *J. Mater. Sci. Technol.*, 26 (2010) 113.
2. S. Moon, Y. Nam, C. Yang and Y. Jeong, *Corros. Sci.*, 53 (2011) 1547.
3. B. Kasalica, S. Stojadinovic, L. Zekovic, I. Belca and D. Nikolic, *Electrochem. Commun.*, 7 (2005) 735.
4. H. Asoh, M. Matsumoto and H. Hashimoto, *Surf. Coat. Technol.*, 378 (2019) 124947.
5. S. Y. Li, J. Wang, Y. Li, X. Q. Zhang, G. Wang and C. W. Wang, *Superlattices Microstruct.*, 75 (2014) 294.
6. L. R. Zhao, J. Wang, Y. Li, C. W. Wang, F. Zhou and W. M. Liu, *Physica B*, 405 (2010) 456.
7. R. X. Wang, L. S. Wang, C. Y. He, M. Lu and L. Sun, *Surf. Coat. Technol.*, 360 (2019) 369.
8. M. Terada, F. M. Queiroz, D. B. S. Aguiar, V. H. Ayusso, H. Costenaro, M. G. Olivier, H. G. Melo and I. Costa, *Surf. Coat. Technol.*, 372 (2019) 422.
9. T. T. Kao and Y. C. Chang, *Appl. Surf. Sci.*, 288 (2014) 654.
10. D. N. Ma, V. Ngo, S. Raghavan and S. Sandoval, *Corros. Sci.*, 164 (2020) 108358.
11. A. S. Mogoda, *Thin Solid Films*, 394 (2001) 173.

12. R. D. Olmo, M. Mohedano, P. Visser, A. Rodriguez, E. Matykina and R. Arrabal, *J. Mater. Res. Technol.*, 15 (2021) 3240.
13. F. Rosalbino, S. Delsante, G. Borzone and E. Angelini, *Corros. Sci.*, 52 (2010) 322.
14. V. K. Sharma, V. Kumar and R. S. Joshi, *J. Mater. Res. Technol.*, 9 (2020) 4919.
15. P. Nezhadi, M. Azadi and M. S. Bahaabad, *Surf. Interfaces*, 18 (2020) 100450.
16. Q. Kuang, Z. W. Lin, W. Lian, Z. Y. Jiang, Z. X. Xie, R. B. Huang and L. S. Zhang, *J. Solid State Chem.*, 180 (2007) 1236.
17. D. Lee, M. Go, S. Son, M. Kim, T. Badloe, H. Lee, J. K. Kim and J. Rho, *Nano Energy*, 79 (2021) 105426.
18. Z. H. Zhang, S. Sridhar, G. Y. Wei, Y. D. Yu, Z. Q. Zhang, L. Jiang, Y. M. Yang, M. W. Shahzad, X. Chen and B. B. Xu, *Surf. Coat. Technol.*, 408 (2021) 126809.
19. N. N. Qiao, Y. L. Nong, N. Liu and Y. Liang, *Mater. Chem. Phys.*, 225 (2019) 458.
20. D. Y. Zhang, G. N. Dong, Y. J. Chen and Q. F. Zeng, *Appl. Surf. Sci.*, 290 (2014) 466.
21. C. K. Chung, K. T. Tu, C. Y. Chang and Y. C. Peng, *Surf. Coat. Technol.*, 361 (2019) 170.
22. J. Oh, Y. W. Jung, J. Lee and Y. Tak, *Stud. Surf. Sci. Catal.*, 146 (2003) 205.
23. M. Iwai and T. Kikuchi, *Electrochim. Acta*, 399 (2021) 139440.
24. M. Moradi and M. Rezaei, *Constr. Build. Mater.*, 317 (2022) 126136.
25. Z. F. Lin, W. Zhang, W. Zhang, L. K. Xu, Y. P. Xue and W. H. Li, *Mater. Chem. Phys.*, 277 (2022) 125503.
26. H. Y. Chen, H. Z. Fan, N. Su, R. Y. Hong and X. S. Lu, *Chem. Eng. J.*, 420 (2021) 130540.
27. X. K. Li and X. Liu, *Int. J. Electrochem. Sci.*, 17 (2022) 220242.

© 2022 The Authors. Published by ESG ([www.electrochemsci.org](http://www.electrochemsci.org)). This article is an open access article distributed under the terms and conditions of the Creative Commons Attribution license (<http://creativecommons.org/licenses/by/4.0/>).